INTERNATIONAL JOURNAL OF HYDROGEN ENERGY 39 (2014) 15735–15745

Available online at www.sciencedirect.com

ScienceDirect

journal homepage: www.elsevier.com/locate/he

EB-PVD deposition of spinel coatings on metallic materials and silicon wafers

Verónica Miguel-Pérez [a], Ana Martínez-Amesti [a,*], María Luisa Nó [b], José Calvo-Angós [c], María Isabel Arriortua [a,*]

[a] Universidad del País Vasco (UPV/EHU), Facultad de Ciencia y Tecnología, Departamento de Mineralogía y Petrología, Sarriena S/N, 48940 Leioa, Vizcaya, Spain

[b] Universidad del País Vasco (UPV/EHU), Facultad de Ciencia y Tecnología, Departamento de Física Aplicada II, Sarriena S/N, 48940 Leioa, Vizcaya, Spain

[c] Institut de Microelectronica de Barcelona (IMB-CNM), CSIC, Campus UAB, 08193 Bellaterra, Barcelona, Spain

ARTICLE INFO

Article history:
Received 3 April 2014
Received in revised form
5 July 2014
Accepted 22 July 2014
Available online 15 August 2014

Keywords:
Metallic materials
Protective coatings
EB-PVD technique
X-ray diffraction (XRD)
Scanning electron microscopy (SEM)

ABSTRACT

Spinel oxides are promising materials as protective coatings on metallic interconnects to reduce the area specific resistance (ASR) at high operating temperature in solid oxide fuel cells (SOFC). In this work, the deposition of $MnCo_2O_4$ (MC) and $MnCo_{1.9}Fe_{0.1}O_4$ (MCF10) materials (1 μm) on Si substrates and commercial alloys (Crofer 22 APU, SS430 and Conicro 4023 W 188) by electron beam physical vapour deposition (EB-PVD) was studied. Optimisation of deposition, the effectiveness of MC and MCF10 protective layers and the influence of the deposition method were investigated after oxidation at 800 °C for 100 h in air. Significant improvements in Cr poisoning of the cathode and in ASR were observed in cells assembled with coated versus uncoated samples. The best results were obtained with cells assembled with MC/Conicro 4023 W 188 with MC deposited by EB-PVD.

Introduction

Solid oxide fuel cells (SOFCs) are an alternative technology to convert chemical energy of fuel gas, such as hydrogen or hydrocarbon fuels, directly into electrical power. One of the main problems affecting the long-term stability of the SOFC stack is degradation of cathode performance by chromium poisoning from metallic interconnects [1–4]. Using a coating that acts as a protective layer can avoid the migration of chromium to the cathode and improve oxide growth resistance of interconnects [5–8].

The coatings must have adequate conductivity, matching thermal expansion, and be chemically compatible with adjacent components and stable in air. Several studies [9–12] have concluded that spinel oxides such as $(Mn, Co)_3O_4$, Co_3O_4, $(Cu, Mn)_3O_4$, $(Mn, Co, Fe)_3O_4$ and/or $(Ni, Co, Mn)_3O_4$, have higher electrical conductivity than oxide scale phases (Cr_2O_3, $(Mn,Cr)_3O_4$) formed under SOFC conditions, and are good candidates to be used as protective layers.

* *Corresponding authors*. Tel.: +34 946015984.
E-mail addresses: ana.martinez@ehu.es (A. Martínez-Amesti), maribel.arriortua@ehu.es (M.I. Arriortua).
http://dx.doi.org/10.1016/j.ijhydene.2014.07.115

Table 1 – Chemical composition of steels samples (in wt %) determined by ICP-AES.

	Cr	Fe	Ni	W	Co	Mn
Crofer 22 APU	22.19 (2)	77.29 (1)	–	–	–	0.52 (1)
SS430	16.77 (2)	82.79 (1)	–	–	–	0.44 (2)
Conicro 4023 W 188	22.07 (1)	2.70 (1)	22.29 (1)	15.50 (2)	36.58 (1)	0.86 (1)

While a variety of techniques have been employed to deposit these kinds of oxides, including electrophoretic deposition [13], magneton sputtering [14], screen printing [15] and electroplating [16], electron beam physical vapour deposition (EB-PVD) has not often been tested. This vacuum deposition technique is a PVD process in which material from a thermal vaporization source reaches the substrate with little or no collision with gas molecules in the space between the source and substrate [17]. The technique has several distinct advantages [18]: high deposition rates; more durable and dense coatings; precise composition control; low contamination; capability for producing multilayered coatings and low temperature deposition. It also allows the composition of the coatings to be changed and for modification of the microstructure by changing process parameters such as time, temperature, pressure and humidity [19–21].

EB-PVD is a versatile technique because it can simultaneously evaporate multiple materials, of different compositions, that are widely employed in modern technologies such as aeronautics, industrial gas turbines, semiconductor manufacture and/or SOFC systems [22–24]. Others studies have shown that the deposition of oxide materials such as $Mn_{1.5}Co_{1.5}O_4$ and MCrAlYO (where M represents a metal, e.g., Co, Mn, Ti or Ni) as coatings on ferritic stainless steels improves long-term ASR stability and decreases Cr volatility [25,26].

The purpose of this work was to extend our previous studies on the behaviour of protective coatings [27], using EB-PVD deposition of $MnCo_2O_4$ (MC) and $MnCo_{1.9}Fe_{0.1}O_4$ (MCF10) on silicon substrates and on metallic materials of different composition (Crofer 22 APU, SS430 and Conicro 4023 W 188). The influence of the deposition method on the behaviour of MC and MCF10 layers on alloys after oxidation at 800 °C for 100 h in air was also investigated.

Experimental

Two Fe–Cr based alloys, Crofer 22 APU (ThyssenKrupp VDM) and SS430 (Hamilton Precision Metals), and a Co based superalloy, Conicro 4023 W 188 (ThyssenKrupp VDM), were used as metallic substrates. Their chemical compositions, determined using inductively coupled plasma with optical emission spectroscopy (ICP-AES) on a Horiba Jobin Yvon Activa spectrophotometer, are shown in Table 1.

The samples were oxidised in air at 800 °C for 100 h in a Carbolite furnace, as described by V. Miguel-Perez et al. [28], to inhibit Fe and Cr transport from the alloys to the protective coating and to avoid the growth of the chromium based layer which increases the interfacial stress [14].

Powdered $MnCo_2O_4$ (MC), $MnCo_{1.9}Fe_{0.1}O_4$ (MCF10) were used as protective coating materials, $La_{0.6}Sr_{0.4}FeO_3$ (LSF40) as cathode material, and $(ZrO_2)_{0.92}$ $(Y_2O_3)_{0.08}$ (YSZ) disks, 25 mm diameter and a thickness of 300 μm, as the electrolyte (NexTech, Fuel Cell Materials) and $Ce_{0.8}Sm_{0.2}O_{1.9}$ (SDC) as the interlayer material between the cathode and the electrolyte (Praxair Surface Technologies).

$MnCo_2O_4$ (MC) and $MnCo_{1.9}Fe_{0.1}O_4$ (MCF10) powders are homogenous and exhibit similar morphology in terms of particle size distribution with an average grain size (d_{50}) of 0.91 and 1.29 μm for MC and MCF10, respectively. The electrical conductivity of MC and MCF10 are 67 and 72 S cm^{-1} at 800 °C in air, respectively [27].

$MnCo_2O_4$ (MC) and $MnCo_{1.9}Fe_{0.1}O_4$ (MCF10) were deposited on Si wafers and pre-oxidised alloys by using EB-PVD in a UNIVEX 450 B e-beam evaporator (Fig. 1a). Prior to deposition, the target samples (MC and MCF10) were prepared by pressing 1 g of the spinel powders at 2 tons for 1 min using a uniaxial

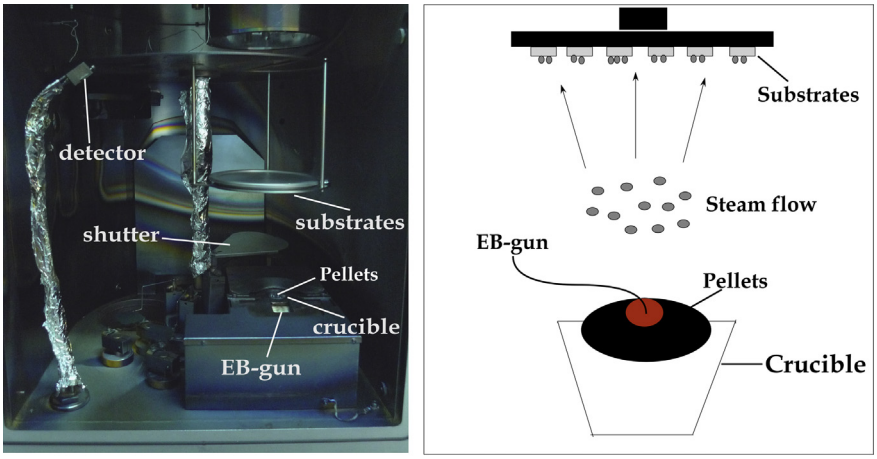

Fig. 1 – a) Photograph of the EB-PVD chamber UNIVEX 450B and b) Schematic diagram of the deposition process by EB-PVD.

press (Specac) with a 13 mm diameter. Pellets were sintered in a conventional Carbolite tubular furnace at 1000 °C for 6 h in air, heating at 3 °C min^{-1}. The substrates (Si wafers and metallic materials) were mounted at an appropriate distance from the evaporation source to reduce radiant heating of the substrate by the vaporization source (Fig. 1b), and the sintered pellets (MC and MCF10) were evaporated in a carbon crucible (~99.9995% C). Deposition was using a standard 6 kW electron beam over the target, with an emission current of ~300 mA. The pressure used during the EB-PVD process was 4×10^{-2} Pa in a reactive oxygen gas atmosphere with 2% Ar.

MC and MCF10 materials were first deposited on monocrystalline silicon wafers of (100) orientation to obtain the temperature and time of recrystallisation. Thermodiffractometry (TDX) analysis was carried out in a Bruker D8 Advance Vantec diffractometer equipped with a variable-temperature stage (HTK 2000) with a Pt sample holder. The power generator was set to 30 kV and 20 mA. The patterns were recorded from room temperature to 800 °C, followed by isothermal oxidation test for 10 h in air, at a heating rate of 3 °C min^{-1}. All patterns were recorded in 2θ steps of 0.033° from 20° to 80°. The surfaces of the metallic material coated with MC and MCF10 deposited by EB-PVD were then characterised by X-ray diffraction (XRD), at room temperature, using a Philips X'Pert Pro automatic diffractometer equipped with Cu K_α radiation ($\lambda = 1.5418$ Å). The power generator was set to 40 kV and 40 mA. The patterns were recorded in 2θ steps of 0.026° in the 20–80° range. Preliminary evaluation of the composition of the oxide surfaces was using X'Pert HighScore Software 2003.

Finally, the coated metallic interconnects (Crofer 22 APU, SS430 and Conicro 4023 W 188) with MC and MCF10 deposited by EB-PVD and symmetrical half-cells (LSF40/SDC/YSZ) were stacked on top of one another for compatibility studies. For better mechanical and electrical contact between the cells and coated metallic interconnects, a dead weight of 1 kg cm^{-2} was placed on top of the stack [27]. For symmetrical half-cell preparation, on both sides of the electrolyte, a samarium doped cerium oxide (SDC) layer and Sr-doped lanthanum ferrite (LSF40) cathode layers were deposited by wet colloidal spray. The SDC layer was first deposited and sintered at 1300 °C for 2 h in air, and then the LSF40 layer was deposited and sintered at 950 °C for 2 h in air to produce a porous layer. The heating-cooling rate throughout the treatment was 3 °C min^{-1}. The suspensions for wet colloidal deposition were made by mixing the powders, ethanol and ZrO_2 cylinders, as grinding media, in a ball mill for 2 h [27].

The cell surfaces in contact with the EB-PVD coated alloys were analysed using an XPS spectrometer (SPECS) to confirm the presence or absence of Cr. All XPS spectra were obtained using a monochromatised X-ray source producing Al K_α radiation ($h\nu = 1.486.6$ eV), and recorded using a SPECS PHOIBOS 150 analyser. The take-off angle of the photoelectrons was 90° with respect to the specimen, with an energy resolution of 0.6 eV. Individual high resolution spectra were obtained at 40 eV. The binding energies (BEs) were calibrated against the surface carbon contamination at 284.6 eV.

For measurement of area specific resistance (ASR), symmetrical half-cells (LSF40/SDC/YSZ), with a 0.25 cm^2 reference electrode area of Pt and coated interconnects (Crofer 22 APU, SS430 and Conicro 4023 W 188), were stacked against each other. A dead weight of 1 kg cm^{-2} was placed on top of the collection of cells to achieve better mechanical contact for conductivity measurements (Fig. 2). Electrical conductivity of the stacks (interconnect/coating/cell) was evaluated with a current density of 0.3 A cm^{-2} and the 3-point technique in air at 800 °C for 100 h using a Solartron 1260 Frequency Response Analyzer.

The microstructure, composition and phase distribution of samples after ASR measurements were analysed using a JEOL JSM-7000F scanning electron microscope (SEM) equipped with a Schottky field emission gun (FEG) and an Oxford Inca Pentafet X3 energy dispersive X-ray analyser (EDX). Surface microstructure was observed using secondary electrons (SE) at an accelerating voltage of 5 kV and a current of 1.96×10^{-11} A. The backscattered electron signal (BSE) at 20 kV and a current intensity of 5.7×10^{-10} A were used for EDX microanalyses. Samples for cross-section analysis were embedded in epoxy resin, polished using standard metallographic techniques, and coated with a coal graphite layer (10 nm), deposited by evaporation (Quorum Q150T Sputter Coater) to provide electrical conductivity.

Results

Characterisation of protective coatings on silicon and on metallic materials

Layers of $MnCo_2O_4$ (MC) and $MnCo_{1.9}Fe_{0.1}O_4$ (MCF10), ~1 μm thick, were deposited on silicon substrates by EB-PVD. By XRD analysis, it was observed that the protective layers were amorphous. Therefore, to determine the temperature at which the spinel oxides begin to crystallise, a TDX study was carried out on coated silicon wafers (Fig. 3), from room temperature to 800 °C in air.

A preliminary qualitative analysis was made to identify the composition of the coating using the Powder Diffraction File (PDF) database [29]. TDX analysis revealed that $MnCo_2O_4$ (MC) and $MnCo_{1.9}Fe_{0.1}O_4$ (MCF10) begin to crystallise at 450 °C in air. An isothermal TDX study was also conducted for 10 h in air (Fig. 4), since 800 °C is the operation temperature for IT-SOFC, to determine stability of the protective layers. In both cases, the qualitative analyses showed that the spinel phases, MC and MCF10, are stable at 800 °C in air.

The surface and cross-section microstructure of ceramic materials (MC and MCF10) deposited on silicon substrates by EB-PVD for different sintering times (1, 10 and 100 h) in air, at

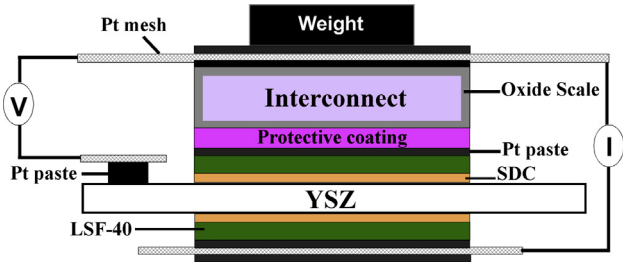

Fig. 2 – Scheme of the setup for the ASR measurements.

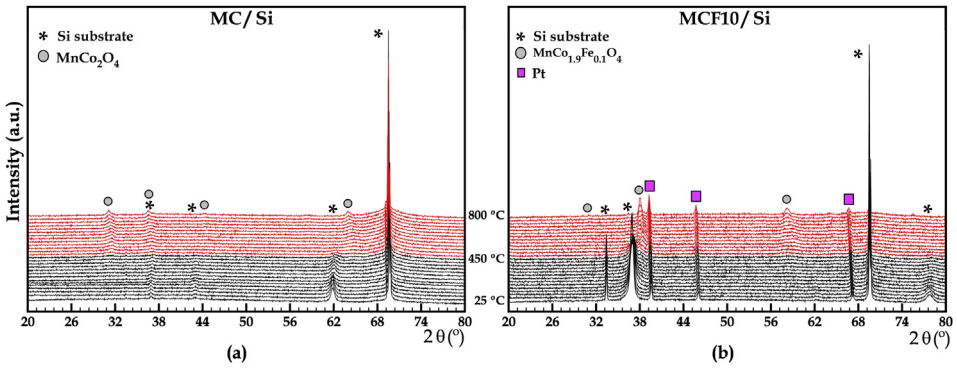

Fig. 3 – X-ray thermodiffractograms for coated Si wafers with (a) MC and (b) MCF10. The Pt peak comes from diffractometer sample holder.

800 °C, were analysed using the secondary electron signal, to investigate the stability and morphology of protective coatings as a function of time (Fig. 5).

After deposition, the surface microstructure of the MC protective coating was homogeneous, with a laminar and fine-grained surface with an average grain size of less than 100 nm, while the MCF10 surface microstructure had two particle morphologies each of different sizes and irregular-shaped. Cross-section images showed a columnar growth, which is more pronounced for MCF10. Both layers had excellent adhesion to Si wafers. After 1 h oxidation, the particles were larger than after deposition, with a size of ~0.25 μm and 0.4 μm for MC and MCF10, respectively. After 100 h, the particle size for MC and MCF10 was greater than after 1 h. There was also a certain amount of porosity of the MCF10 layer after 100 h, possibly due to the presence of Fe in the spinel structure. In contrast, the difference in microstructure between MCF10 and MC is because $MnCo_{1.9}Fe_{0.1}O_4$ is a solid solutionmix of $MnCo_2O_4$ and $MnFe_2O_4$ spinels which have different processes of evaporation and crystallisation [30,31].

After these analyses, 1 μm of the protective coatings was deposited, using EB-PVD, on pre-oxidised interconnects and sintered at 800 °C for 1 h to obtain dense, crystalline coatings. The chemical reactions and mechanical stability between the alloys and the applied layers were analysed using XRD and SEM. Fig. 6 shows the X-ray patterns, taken at room temperature after 1 h at 800 °C in air, on the surface of MC and MCF10 coated on metallic substrates.

Qualitative X-ray diffraction revealed the formation of a spinel phase with different composition and the presence of Cr_2O_3 oxide formed during the pre-oxidation and oxidation processes. This phase (Cr_2O_3) was detected as the deposited layers were 1 μm thick and the penetration of X-rays is higher than 1 μm. This compound is part of the oxide scale formed in this kind of metallic material after oxidation. Generally, these oxide scales have a double-layer structure of chromia (Cr_2O_3) and a spinel phase composed of $(Fe, Cr, Mn)_3O_4$ [32].

The microstructure of the surfaces of the MC and MCF10 coating on the alloys and the cross-section EDX elemental line-scan of the samples after heat treating at 800° C for 1 h was analysed by SEM (Fig. 7).

The surface microstructures of the protective layers on alloys differed. The reason may be that the composition of the oxide scale formed in each alloy differed after pre-oxidation. These oxide scales may also react with the deposited spinel layers, forming other oxides with different morphologies.

The surface morphology of Crofer 22 APU coated with MC was homogeneous, with pyramidal, geometrical particles of 1 μm, while the surface of MCF10 had agglomerates of smaller particles of different sizes. However, the surface of protective layers on SS430 and Conicro 4023 W 188 were homogeneous

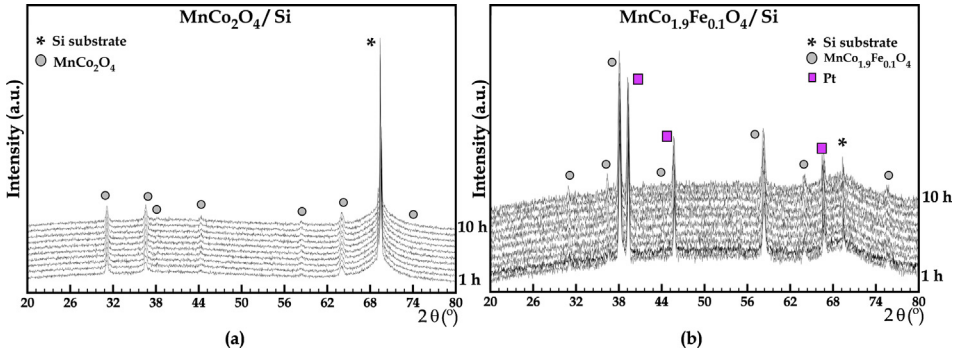

Fig. 4 – X-ray isothermal test for coated Si wafers with (a) MC and (b) MCF10 at 800 °C in air from 1 h to 10 h. The Pt peak comes from diffractometer sample holder.

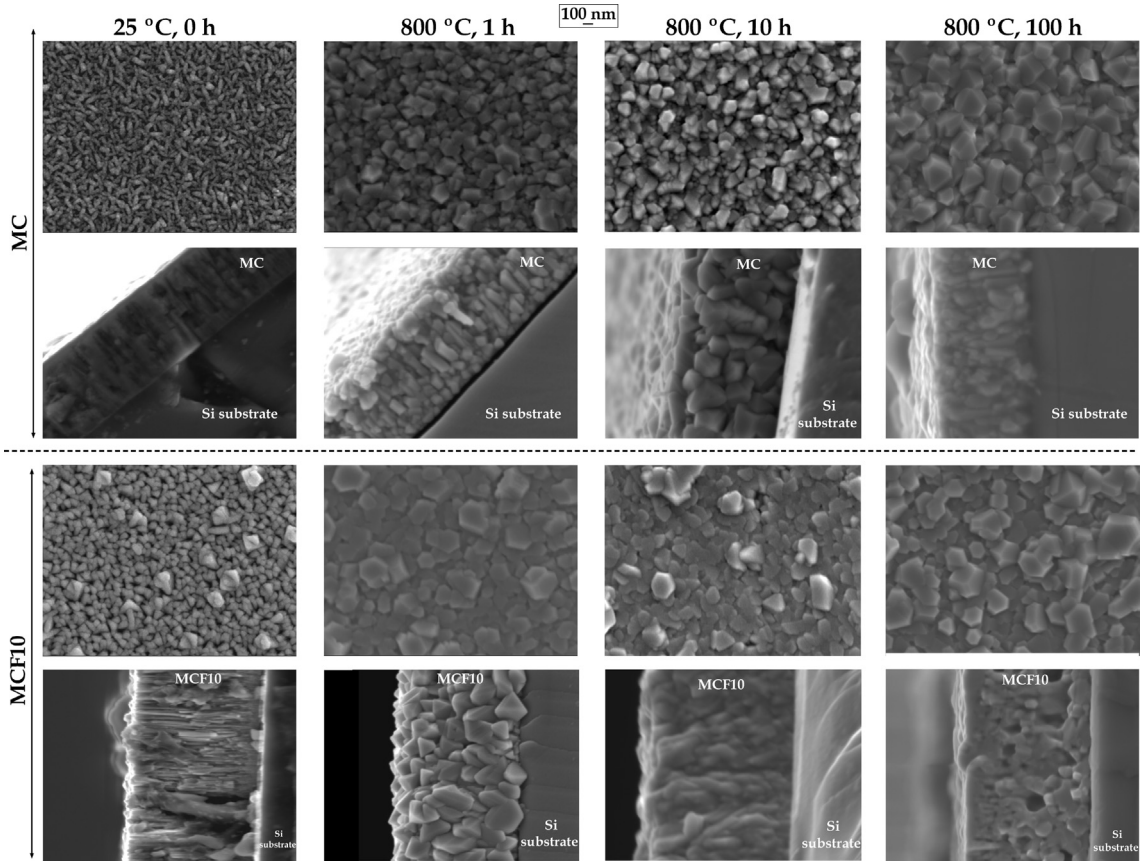

Fig. 5 – SEM micrographs of $MnCo_2O_4$ (MC) and $MnCo_{1.9}Fe_{0.1}O_4$ (MCF10) coated on Si substrates after deposition and oxidation at 800 °C for 1, 10 and 100 h in air.

with polycrystalline nodules. Other research groups [33,34] have observed similar morphologies as a result of the reaction between $MnCo_2O_4$ (MC) and chromia (Cr_2O_3), forming phases such as $Mn_{0.65}Co_{0.35}Cr_2O_4$ and $Mn_{1.84}Co_{1.04}Cr_{0.12}O_4$.

The oxide scale formed on SS430 and Conicro 4023 W 188 had higher amounts of chromia than Crofer 22 APU after oxidation at 800 °C for 1 h in air, as found by V. Miguel-Perez et al. [28]. As a result, the morphology of the particles on the

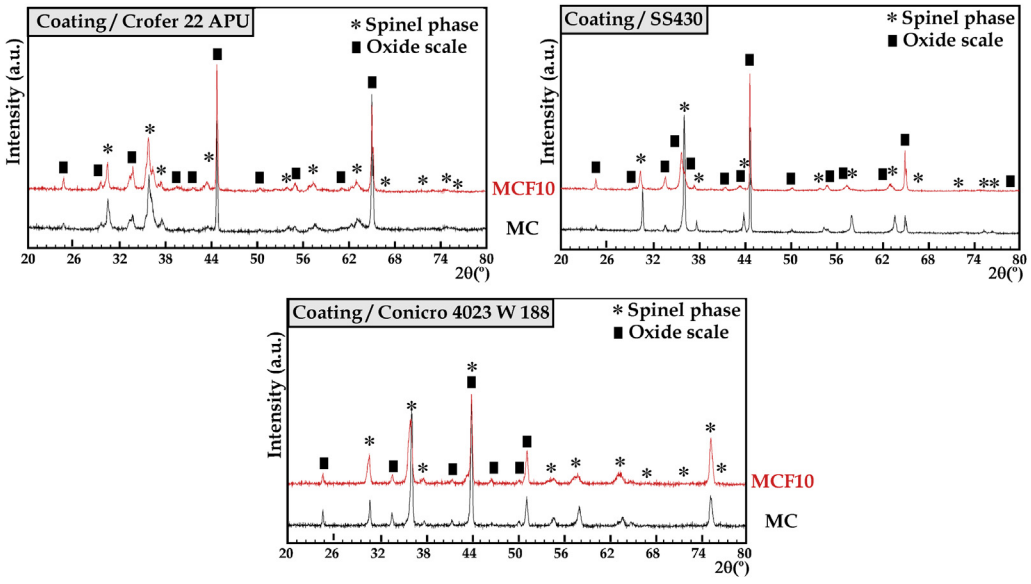

Fig. 6 – XRD patterns of pre-oxidised interconnects (Crofer 22 APU, SS430 and Conicro 4023 W 188) coated with MC and MCF10 by EB-PVD after 1 h at 800 °C in air.

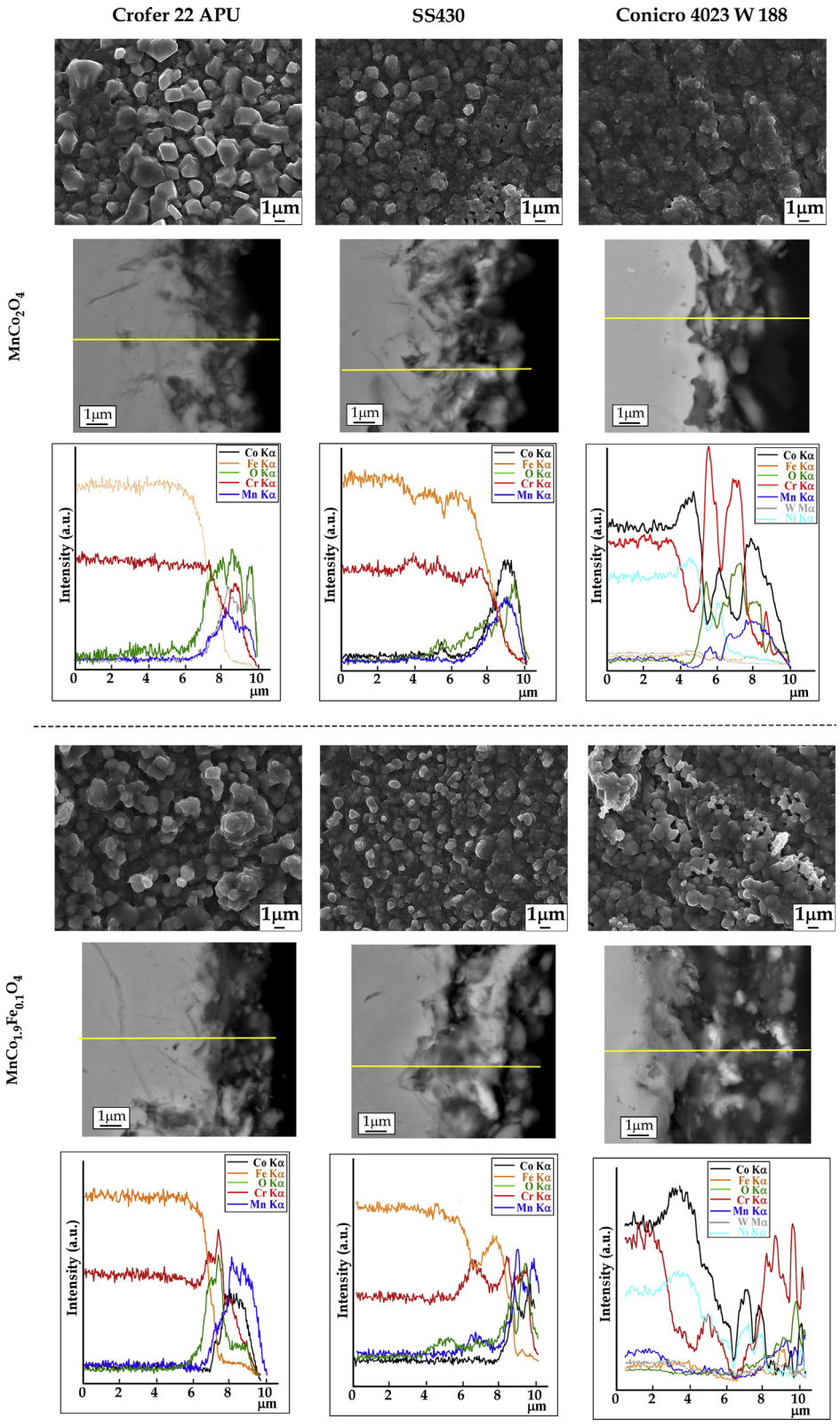

Fig. 7 – SEM micrographs of the surface $MnCo_2O_4$ (MC) and $MnCo_{1.9}Fe_{0.1}O_4$ (MCF10) coated by EB-PVD on alloys and cross section EDX elemental line scan after oxidation at 800 °C for 1 h in air.

surface of Crofer 22 APU (Fig. 7) differed from that of the particles formed on SS430 and Conicro 4023 W 188.

The cross-section of the elemental EDX line-scan showed that the oxide layer on Crofer 22 APU, SS430 and Conicro 4023 coated with MC and MCF10 was composed of particles with different compositions. The whiter particles were mainly Cr and the greyer ones Cr, Mn and Co. Some Fe was present when MCF10 was used as the protective layer. These particles may be

those with spinel structure, in agreement with the XRD analyses. The more homogeneous oxide layer was that formed on MC/Crofer 22 APU, composed only of Cr, Mn and Co.

Compatibility between protective layers and the LSF40 cathode

A compatibility study between protective coatings and the cathode material (LSF40) was made to verify that diffusion of chromium was reduced through the LSF40 cathode by the deposition of MC and MCF10 on the metallic interconnects. In this study, the surface of a multilayer cell was investigated by XPS after 100 h, at 800 °C, in contact with the different interconnects coated with MC and MCF10. Fig. 8 shows the high-resolution Cr-2p spectra of the cell surfaces. All core-level intensities were corrected for XPS sensitivity factors and plotted as a function of the binding energy (BE).

For all samples, the XPS spectra showed a doublet near the BEs of ~579.0 and 589.3 eV (Cr-$2p_{3/2}$ level), suggesting the presence of Cr^{6+}. However, the lower BE positions of 576.5 and 586.6 eV correspond to Cr^{3+}. The +6 valence of the Cr ion in uncoated samples indicates the existence of segregated phases such as CrO_3 or $SrCrO_4$ [35], whereas the +3 valence corresponds to the Cr of the chromia (Cr_2O_3) phase. The intensity of the chromium signal indicates the amount of this element in the different samples. The results show there were more Cr deposits on the cathode surface in contact with uncoated alloy than with the coated alloys.

Stack performance

The electrical performance of the stack with Crofer 22 APU, SS430 and Conicro 4023 W 188 coated with MC and MCF10 was evaluated using ASR measurements in air at 800 °C. Fig. 9 shows the contact ASR as a function of time, of stacks formed by cell (LSF40/SDC/YSZ) and selected metallic interconnects EB-PVD-coated with MC and MCF10 protective layers. To evaluate the efficiency and the effect of deposition method, the ASR values obtained were compared with ASR values obtained for stacks formed by cell and interconnect coated, with MC and MCF10, by the wet colloidal method [27]. Reference ASR values of alloys assembled with uncoated interconnect are also shown (Fig. 9).

The ASR values of cells assembled with uncoated alloys were higher than those of stacks with the interconnect coated with MC and MCF10. This may be due to Cr-poisoning of the cathode. The value of ASR of the cell assembled with uncoated Conicro 4023 W 188 was similar to that of the cell/MC/Conicro 4023 W 188 sintered for 10 h and deposited by the wet colloidal method. This could be due to the formation of secondary phases such as (Co, Cr, Mn)$_3O_4$ and (Fe, Cr, Mn)$_3O_4$ between cells and uncoated Conicro 4023 W 188, which have a similar electrical conductivity to deposited spinel oxides.

In general, for all stacks, the contact ASR was lower when the protective layer was deposited by EB-PVD. The cells assembled with the coated MCF10/Crofer 22 APU where MCF10 was deposited by EB-PVD had higher ASR values than stacks in which MCF10 was deposited by the wet colloidal method. A possible explanation is that, when MCF10 is deposited on Crofer 22 APU by EB-PVD, the (Mn, Cr, Fe)$_3O_4$ spinel phase is mainly formed in the recrystallisation process, and it has lower electrical conductivity than MCF10.

On the other hand, although SS430 is also a Fe–Cr-based alloy, like Crofer 22 APU, the contact ASR values are very different, being higher for cells with coated SS430. The SS430 had lower oxidation resistance and the composition of the oxide scale formed in the pre-oxidation process differed, such that the compatibility between the oxide scale and protective layers deposited by EB-PVD also differed [27].

In addition, the ASR value of the cell/MCF10/Conicro 4023 W 188 stack where MCF10 was deposited by EB-PVD (1.150 mΩ cm^2), was similar to that of the stack formed by wet colloidal spray (1.114 mΩ cm^2). Finally, the lowest ASR value was for the stack formed by cell/MC/Conicro 4023 W 188 (0.589 mΩ cm^2), where MC was deposited by EB-PVD. This may be because the electrical conductivity of the oxides formed in the MC recrystallisation process was greater than for those formed in Crofer 22 APU and SS430.

In order to better understand these results, the microstructure and Cr distribution along the MC and MCF10 coating deposited by EB-PVD was analysed. EDX line scan analysis was performed on a cross-section of the coated alloys (Crofer 22 APU, SS430 and Conicro 4023 W 188) after ASR measurement (Fig. 10).

In the EDX analyses, three layers were distinguished for all except the MCF10/SS430 system, in which there were four

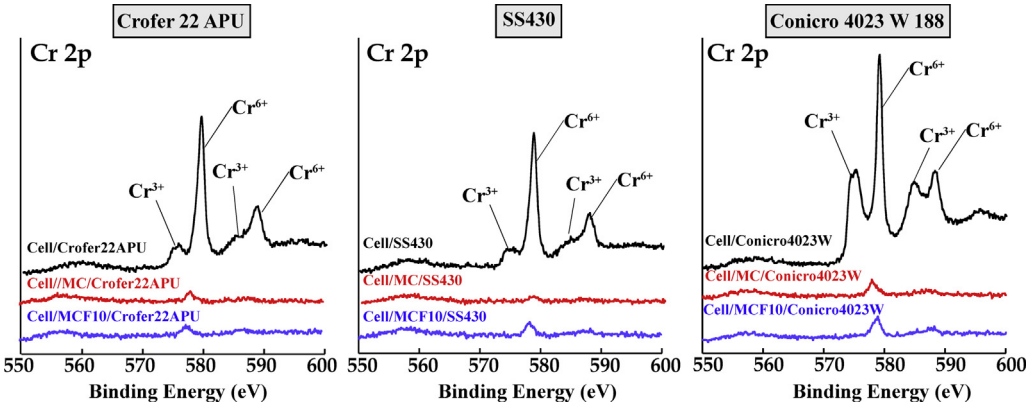

Fig. 8 – XPS spectra of Cr-2p for cells surface in contact with coated interconnects by EB-PVD after oxidation at 800 °C for 100 h in air. XPS spectra of Cr-2p for cells surface in contact with uncoated alloys as reference have been included.

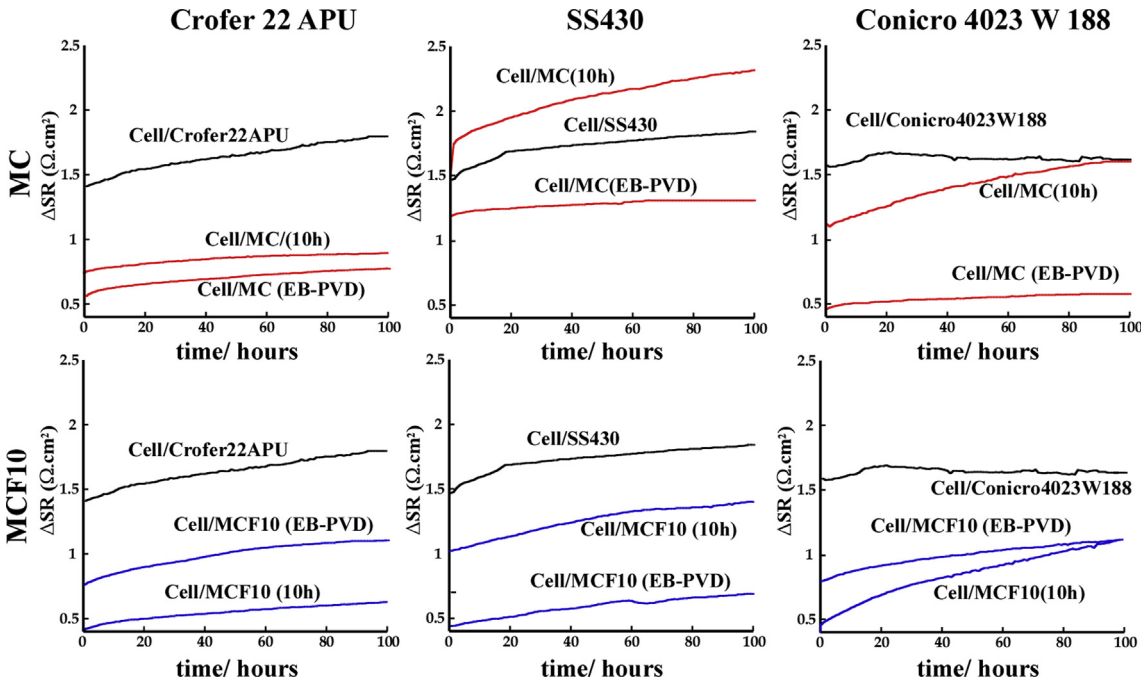

Fig. 9 – ASR measurement of cell with Crofer 22 APU, SS430 and Conicro 4023 W 188 uncoated and coated with MC and MCF10 by wet colloidal spray (1000 °C, 10 h) and EB-PVD (800 °C, 1 h) at 800 °C for 100 h in air.

layers. For all samples, area I is the metallic substrate, area II the oxide layer composed of the scale formed during oxidation (Cr_2O_3, $(Mn,Cr)_3O_4$) and the ~1 μm protective layer deposited by EB-PVD. For the MCF10/SS430 system, area III was an oxide layer with different composition to area II. Finally, area IV for the MCF10/SS430 system and area III (for systems with three areas), was the Pt paste used to make the electrical contact.

In the MC/Crofer 22 APU and MCF10/Crofer 22 APU systems, area II had a thickness of approximately 3–3.5 μm, composed mainly of Cr, O, Mn and some Fe. The area II of the MCF10/Crofer 22 APU system contained a mix of the oxide scale formed during the pre-oxidation and the protective layer deposited by EB-PVD, composed mainly of Mn, Co, O, Cr and Fe.

Area II of the MCF10/SS430 system was composed of Cr, Fe, O and some Mn, with a thickness of ~23 μm, and area III was composed of a mix of Fe_2O_3/Fe_3O_4, with a thickness of ~24 μm. The exhaustive oxidation in this system could be due to the MCF10 material not being a good protective layer for alloys with high Fe content, as it does not prevent the formation of Fe_2O_3/Fe_3O_4. In addition, area II in the MC/SS430 system was composed mainly of Cr, Mn, Co and O and some Fe.

In the MC/Conicro 4023 W 188 system, the amount of Cr decreased in area I, and increased in area II. The oxide scale was also thinner in this system, with a higher amount of Cr than the MCF10/Conicro 4023 W 188 system.

When the EDX analyses shown in Figs. 7 and 10 are compared, the thickness of the oxide layer was ~1 μm in all cases except for the MCF10/SS430 system, after 100 h at 800 °C. The density of the coatings deposited on alloys by EB-PVD was also found to become denser over time but the composition was heterogeneous. This is because of the different in the chemical composition of the oxide scale formed during the pre-oxidation process in the alloy, and because the reactivity between the oxide scale and the MC and MCF10 protective layer differed during recrystallisation and over oxidation time.

Discussion

The systems with $MnCo_2O_4$ (MC) and $MnCo_{1.9}Fe_{0.1}O_4$ (MCF10) as the protective layer between cell and interconnects had lower ASR values than the systems without these materials, due to the reduction of chromium diffusion. The electrochemical results were dependent on the metallic (Crofer 22 APU, SS430 and Conicro 4023 W 188) and ceramic materials (MC and MCF10) used for the protective layer and on the deposition method.

Of the systems studied, the more promising are cell/MC/Conicro 4023 W, where EB-PVD was used for MC deposition (0.589 mΩ cm^2), and cell/MCF10/Crofer 22 APU by wet colloidal spray sintered at 1000 °C for 10 h in air (0.637 mΩ cm^2). Crofer 22 APU and Conicro 4023 W 188 have high corrosion resistance due to the higher chromium content and reactive elements (Mn, W, Si, Cu, Al, La and Ti) which improve the oxide scale growth [28]. Chromium diffusion through LSF40 cathode is also lower.

The cell/MC/Conicro 4023 W 188 by EB-PVD had the lowest ASR value. This was due to the higher electrical conductivity of the oxide scale, with good compatibility with ceramic oxides deposited by EB-PVD, by the formation of Laves phases which reduced the oxide scale growth. In addition, Cr migrated from the alloy interacted with protective layers and generated a $MnCoCrO_4$ spinel phase, which has higher electrical conductivity than that of Cr_2O_3 [36].

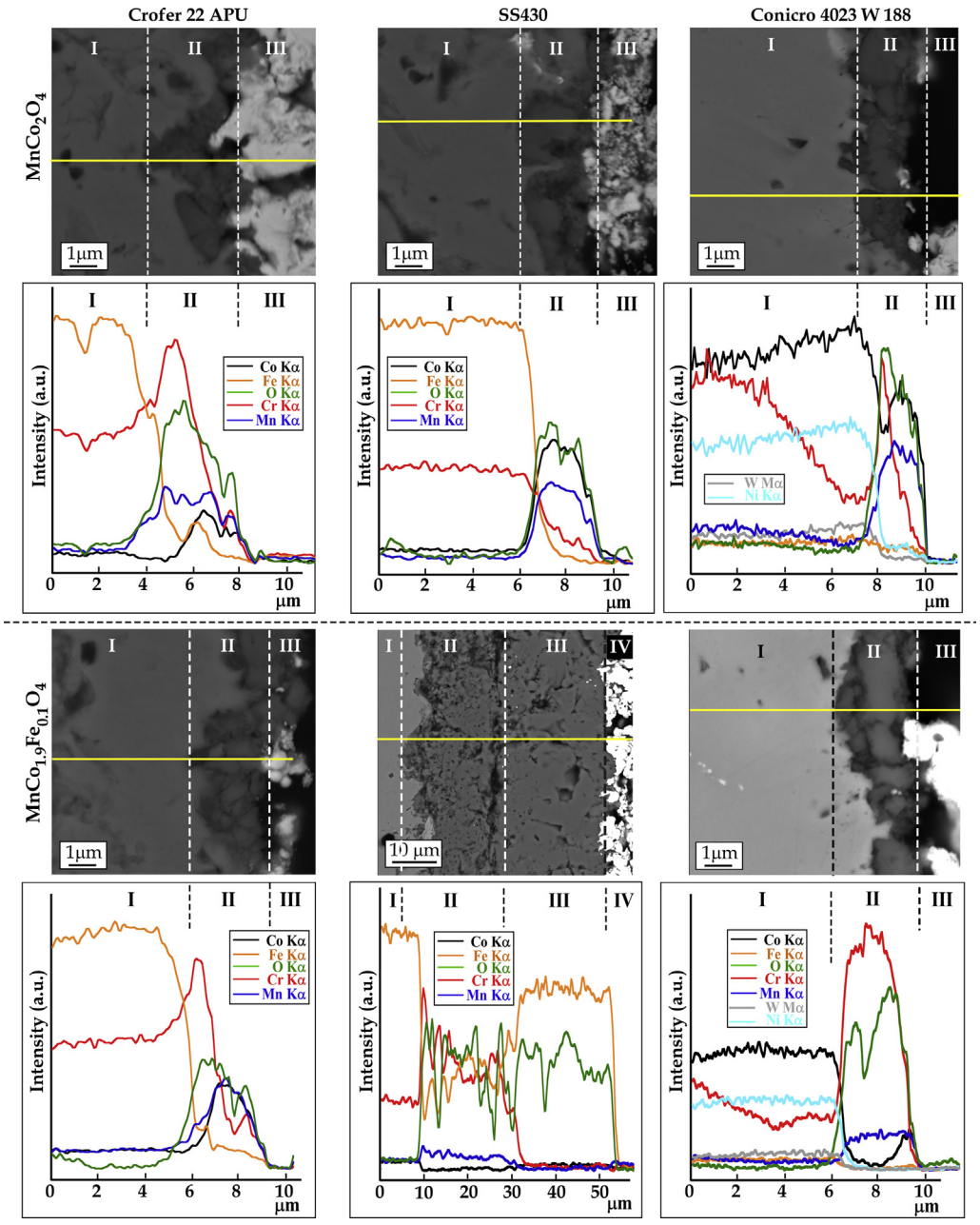

Fig. 10 – Cross section BSE images and corresponding EDX elemental line scan of LSF40 in contact with coated alloys with MC and MCF10 at 800 °C in air for 100 h. Acquisition for line scan: 20 kV, 25% dead time, 5 steps with 77 s/step.

There are studies in which $(Mn, Co)_3O_4$ and $(Mn, Co, Fe)_3O_4$ coatings have been deposited by electrophoretic deposition [13], magneton sputtering [14], screen printing [15] and HVOF spraying [37]. In all cases an improvement in oxide scale growth and prevention of chromium migration through perovskite materials was observed. The thickness of the layers was about 10 µm. This means that, MC and MCF10 deposition by EB-PVD requires less material to achieve the same result, so reducing costs.

In general, the results indicate a correlation between the sintering conditions, the oxidation of interconnects and electrical resistance with the formation of secondary phases under SOFC conditions. The systems formed with MC and MCF10 protective layers deposited by EB-PVD exhibited a lower ASR and less LSF40 poisoning.

Conclusions

This work describes the effect of the deposition method of two protective coatings on three metallic interconnects for IT-SOFC. It demonstrates that electron beam physical vapour deposition (EB-PVD) is an effective technique to obtain dense $MnCo_2O_4$ (MC) and $MnCo_{1.9}Fe_{0.1}O_4$ (MCF10) layers on Crofer 22 APU, SS430 and Conicro 4023 W 188 alloys.

The ceramic coatings deposited by EB-PVD showed a different morphology depending on the alloy used and the reactivity between the oxide scale and the deposited spinel oxides. MC deposited by EB-PVD gave the best electrochemical results with Conicro 4023 W 188, whereas lower values of ASR with MCF10 were obtained on the Fe–Cr-based alloys, Crofer 22 APU and SS430.

EB-PVD application of MC and MCF10 spinel as protective layers acted as an effective barrier to avoid the diffusion of Cr through the LSF40 cathode material. The most promising stack was found to be cell/MC/Conicro 4023 W 188.

Acknowledgement

This work has been financially supported by the Ministerio de Ciencia e Innovación (MAT2010-15375 and Consolider-Ingenio 2010 CSD2009-00013), by Dpto. Industria, Innovación, Comercio y Turismo (SAIOTEK 2013 programme) and by Dpto. Educación, Política Lingüística y Cultura (IT-630-13) of the Basque Government. The authors wish to thank Ikerlan's Fuel Cell group (Miñano, Álava) and the technical and human support provided by SGIker-UPV/EHU. Prof. F. Campabadal (IMB-CNM) is acknowledged for useful scientific discussions. V. Miguel-Pérez wishes to thank UPV/EHU for funding.

REFERENCES

[1] Jacobson AJ. Materials for solid oxide fuel cells. Chem Mater 2010;22:660–74.
[2] Hilpert K, Quaddakers WJ, Singheiser L. In: Vielstich W, Gasteiger HA, Lamm A, editors. Handbook of fuel cells-fundamentals, technology and applications, vol. 4. New Jersey, USA: John Wiley & Sons; 2003. p. 1037–51.
[3] Horita T, Xiong Y, Kishimoto H, Yamaji K, Brito ME, Yokokawa H. Chromium poisoning and degradation at $(La,Sr)MnO_3$ and $(La,Sr)FeO_3$ cathodes for solid oxide fuel cells. J Electrochem Soc 2010;157:B614–20.
[4] Jiang SP, Chen X. Chromium deposition and poisoning of cathodes of solid oxide fuel cells – a review. Int J Hydrogen Energy 2014;39:505–31.
[5] Liu Y, Fergus JW, Cruz CD. Electrical properties, cation distributions, and thermal expansion of manganese cobalt chromite spinel oxides. J Am Ceram Soc 2013;96:1841–6.
[6] Shaigan N, Qu W, Ivey DG, Chen W. A review of recent progress in coatings, surface modifications and alloy developments for solid oxide fuel cell ferritic stainless steel interconnects. J Power Sources 2010;195:1529–42.
[7] Person AH, Mikkelsen L, Hendriksen PV, Somers MAJ. Interaction mechanisms between slurry coatings and solid oxide fuel cell interconnect alloys during high temperature oxidation. J Alloys Compd 2012;52:16–29.
[8] Frotzheim J, Canovic S, Nikuma M, Sachitanand R, Johansson V, Svensson JE. Long term study of Cr evaporation and high temperature corrosion behaviour of Co coated ferritic steel for solid oxide fuel cell interconnects. J Power Sources 2012;220:217–27.
[9] Jalilvand G, Faghihi-Sani MA. Fe doped Ni–Co spinel protective coating on ferritic stainless steel for SOFC interconnect application. Int J Hydrogen Energy 2013;38:12007–14.
[10] Magdefrau NJ, Chen L, Sun EY, Yamanis J, Aindow M. Formation of spinel reaction layers in manganese cobaltite coated Crofer 22 APU for solid oxide fuel cell interconnects. J Power Sources 2013;227:318–26.
[11] Dayagui AM, Askari M, Gannon P. Pre-treatment and oxidation behavior of sol–gel Co coating on 430 steel in 750 °C air with thermal cycling. Surf Coat Technol 2012;206:3495–500.
[12] Montero X, Tietz F, Sebold D, Buchkremer HP, Ringuede A, Cassir M, et al. $MnCo_{1.9}Fe_{0.1}O_4$ spinel protection layer on commercial ferritic steels for interconnect applications in solid oxide fuel cells. J Power Sources 2008;184:172–9.
[13] Yoo J, Woo SK, Yu JH, Lee S, Park GW. $La_{0.8}Sr_{0.2}MnO_3$ and $(Mn_{1.5}Co_{1.5})O_4$ double layer coated by electrophoretic deposition on Crofer22 APU for SOEC interconnect applications. Int J Hydrogen Energy 2009;34:1542–7.
[14] Hoyt KO, Gannon PE, White P, Tortop R, Ellingwood BJ, Khoshuei H. Oxidation behavior of $(Co,Mn)_3O_4$ coatings on preoxidized stainless steel for solid oxide fuel cell interconnects. Int J Hydrogen Energy 2012;37:518–29.
[15] Montero X, Jordan N, Pirón-Abellán J, Tietz F, Stöver D, Cassir M, et al. Spinel and perovskite protection layers between Crofer22APU and $La_{0.8}Sr_{0.2}FeO_3$ cathode materials for SOFC interconnects. J Electrochem Soc 2009;156:B188–96.
[16] Liu Y, Chen D. Protective coatings for Cr_2O_3-forming interconnects of solid oxide fuel cells. Int J Hydrogen Energy 2009;34:9220–6.
[17] Mattox DM. Handbook of physical vapor deposition (PVD) proccessing. 2nd. Oxford: Elsevier; 2010.
[18] Singh J, Wolfe DE. Review: nano and macro-structured component fabrication by electron beam-physical vapor deposition (EB-PVD). J Mater Sci 2005;40:1–26.
[19] He XD, Xin Y, Li MW, Sun Y. Microstructure and mechanical properties of ODS Ni-based superalloy foil produced by EB-PVD. J Alloys Compd 2009;467:347–50.
[20] Mohite KC, Khollam YB, Mandale AB, Patil KR, Takwale MG. Characterization of silicon oxynitride thin films deposited by electron beam physical vapor deposition technique. Mater Lett 2003;57:4170–5.
[21] Schulz U, Schmücker M. Microstructure of ZrO_2 thermal barrier coatings applied by EB-PVD. Mater Sci Eng a 2000;276:1–8.
[22] Sun Y, Lin X, He X, Zhang J, Li M, Song G, et al. Effects of substrate rotation on the microstructure of metal sheet fabricated by electron beam physical vapor deposition. Appl Surf Sci 2009;255:5831–6.
[23] Baek S, Prabhu V. Simulation model for an EB-PVD coating structure using the level set method. J Manufac Process 2009;11:1–7.
[24] Creus J, Berziou C, Cohendoz S, Perez V, Rebere C, Reffass V, et al. Reactivity classification in saline solution of magnetron sputtered or EBPVD pure metallic, nitride and Al-based alloy coatings. Corros Sci 2012;57:162–73.
[25] Gannon P, Deibert M, White P, Smith R, Chen H, Priyantha W, et al. Advanced PVD protective coatings for SOFC interconnects. Int Hydrogen Energy 2008;33:3991–4000.
[26] Gorokhovsky VI, Gannon PE, Deibert MC, Smith RJ, Kayani A, Kopczyk M, et al. Deposition and evaluation of protective PVD coatings on ferritic stainless steel SOFC interconnects. J Electrochem Soc 2006;153:A1886–93.
[27] Miguel-Pérez V, Martínez-Amesti A, Nó ML, Larrañaga A, Arriortua MI. The effect of doping $(Mn,B)_3O_4$ materials as protective layers in different metallic interconnects for solid oxide fuel cells. J Power Sources 2013;243:419–30.
[28] Miguel-Pérez V, Martínez-Amesti A, Nó ML, Larrañaga A, Arriortua MI. Oxide scale formation on different metallic interconnects for solid oxide fuel cells. Corros Sci 2012;60:38–49.

[29] Pfoertsch DE, McCarthy GI. ICDD grant-in-aid. University Park, Pennsylvania, USA: Penn State University; 1977.
[30] Sauchuk V, Kusnezoff M, Trofimenko N, Megel S, Baldus H-P, Reinert A. Development of effective protective materials for SOFC metallic interconnects. In: Proceedings of the 8th European SOFC forum, 31 Junio-4 Julio, Lucerne, Switzerland; 2008.
[31] Petric A, Ling H. Electrical conductivity and thermal expansion of spinels at elevated temperatures. J Am Ceram Soc 2007;90:1515–20.
[32] Miguel-Pérez V. Interconectores metálicos y capas protectoras para su aplicación en pilas SOFC. PhD Thesis. Spain, Bizkaia: UPV/EHU; 2013.
[33] Wang K, Liu Y, Fergus JW. Interactions between SOFC interconnect coating materials and chromia. J Am Ceram Soc 2011;94:4490–5.
[34] Mardare CC, Spiegel M, Savan A, Ludwig A. Thermally oxidised Mn-Co thin films for application as protective coatings for SOFC interconnects. J Electrochem Soc 2009;156(2):B1431–9.
[35] Machet A, Galtayries A, Marcus P, Combrade P, Jolivet P, Scoot P. XPS study of oxides formed on nickel-base alloys in high-temperature and high-pressure water. Surf Interf Anal 2002;34:197–200.
[36] Fang Y, Wu C, Duan X, Wang S, Chen Y. High-temperature oxidation process analysis of $MnCo_2O_4$ coating on Fe-21Cr alloy. Int J Hydrogen Energy 2011;36:5611–6.
[37] Thomann O, Pihlatie M, Rautanen M, Himanen O, Lagerbom J, Mäkinen M, et al. Development and application of HVOF sprayed spinel protective coating for SOFC interconnects. J Therm Spray Technol 2013;22:631–9.